J Mater Sci (2009) 44:4806–4813
DOI 10.1007/s10853-009-3732-0

Thermal- and stress-induced lattice distortions in a single Kevlar49 fibre studied by microfocus X-ray diffraction

R. J. Davies · M. Burghammer

Received: 24 April 2009 / Accepted: 6 July 2009 / Published online: 25 July 2009
© Springer Science+Business Media, LLC 2009

Abstract Understanding the macroscopic physical and mechanical properties of poly(*p*-phenylene terephthalamide) (PpTA) fibres as a function of temperature requires an understanding of how temperature influences its microscopic structure. This study investigates lattice distortions in single PpTA fibres using the high brilliance of a synchrotron radiation microbeam. Lattice distortions are studied over a temperature range of 110–350 K and the influence of tensile deformation is also considered. The results reveal linear thermal expansion behaviour for all unit cell axes, in general agreement with literature. Expansion/contraction is greatest along the [100] direction whilst being reduced along [010] by inter-chain hydrogen bonding. During macroscopic deformation, longitudinal crystal strain dominates with respect to axial lattice distortions induced by temperature changes. There is only a small change in the [100] coefficient of thermal expansion, with the [010] and [001] directions being largely unaffected.

Introduction

The high-performance polymeric fibre poly(*p*-phenylene terephthalamide), or PpTA, is renowned for its remarkable mechanical properties and environmental resistance. In particular, it can tolerate a comparatively wide temperature range compared to most other polymers, and with only a moderate decrease in performance. With a thermal degradation temperature of around 450 °C [1], many applications could exploit these properties. At the exotic end of the application spectrum, studies report on potential uses as mechanical supports in space-borne refrigerators and fan containment systems in supersonic jet engines [2, 3]. At the more mundane end, meanwhile, heat-resistant PpTA gloves are already widely available.

Aside from specialist high- and low-temperature applications, the dimensional stability of PpTA as a function of temperature is of critical importance to the composites industry. In order to avoid residual stresses during the manufacture of certain composite materials, it is necessary to match the coefficient of thermal expansion between the reinforcing fibres and matrix. Similar consideration needs to be given to composite applications which demand a tolerance for temperature changes during use. For example, the aerospace industry has become one of the largest consumers of composite materials due to their environmental resistance, formability and impressive strength-to-weight ratio. For such applications it is critical to ensure that heterogeneous dimensional changes due to variations in thermal expansion do not degrade the mechanical performance of the material.

In order to fully exploit the temperature resistance of PpTA and ensure its safe use in composites, it is necessary to understand how its physical and mechanical properties change as a function of temperature. Although most applications are ultimately concerned only with macroscopic properties, the first step towards this goal is to understand how temperature influences PpTA on a micro-structural level. Whilst a number of early studies reported on the bulk coefficient of thermal expansion for PpTA [4, 5], Ii et al. [6] were the first to consider microstructural effects using X-ray diffraction. By heating bundles of fibres up to 600 K, distortions of the crystal lattice could be monitored and the combined effects of temperature and remote stresses investigated [6, 7]. Since then, the coefficient of thermal

R. J. Davies (✉) · M. Burghammer
European Synchrotron Radiation Facility, 6 rue Jules Horowitz, 38043 Grenoble Cedex, France
e-mail: rdavies@esrf.fr

expansion of the PpTA crystal lattice has been further studied at both high and low temperatures [8, 9]. It has also been calculated based upon finite temperature simulations [10]. Despite this body of work, there are still considerable differences in the values reported between the different studies and a number of unanswered questions remain.

Microfocus X-ray diffraction (microdiffraction) is now considered to be a routine tool for characterising single fibres and has been employed extensively for studying PpTA [11–13]. For example, microdiffraction has revealed skin–core microstructural variations across single PpTA fibres [13]. It has also been coupled with in situ deformation to investigate structure–property relationships [12]. This preliminary study reports on the extension of microdiffraction to monitor PpTA crystal lattice distortions due to variations in temperature. The same variations will also be investigated as a function of applied remote stress. This can be achieved by performing Wide-angle X-ray Scattering (WAXS) in combination with in situ cryogenic cooling/heating and deformation. The use of a high brilliance synchrotron radiation microbeam allows such studies to be carried out on single fibres. This reduces the averaging effects which are inherent to the use of fibre bundles and allows for a dynamic, rather than static, data collection strategy.

Experimental

Materials

The Kevlar49 variety of PpTA is reported on in this study. Kevlar49 is manufactured by DuPont (USA), and has a reported modulus and strength of 113 and 2.4 GPa, respectively [14].

Cryo-deformation coupled with microdiffraction

Microdiffraction was carried out at the ID13 microfocus beamline of the European Synchrotron Radiation Facility (ESRF). The beamline was configured with a monochromatic beam ($\lambda \approx 0.1$ nm), focalised using a pair of crossed Kirkpatrick Baez mirrors. The resulting beam spot size at the focal position was approximately 1 μm in both the horizontal and vertical directions. A single PpTA fibre of 50 mm gauge length was mounted at the X-ray beam's focal position within a custom-built deformation rig. The deformation rig consists of a load cell and linear translation stage which can be operated remotely by RS-232. An OxfordCryosystems Cryostream 700 series was also mounted within the beamline sample environment for locally heating and cooling the PpTA sample. The Cryostream has a temperature range of 80–500 K and a temperature stability of 0.1 K.

Prior to the start of X-ray data collection the PpTA fibre was preconditioned by cooling to 110 K and then reheating to room temperature at a rate of 350 K/h. This procedure is necessary to eliminate hysteresis effects due to thermal annealing, as reported in a number of previous studies [6, 9].

Microfocus X-ray diffraction data were collected using a 16-bit FReLoN CCD detector with an average pixel size of 52.5 μm. All diffraction data were acquired at a sample-to-detector distance of 76.8 mm. Exposure times of 10 s were used, with temperature, force and strain information recorded for each acquisition. Figure 1 shows a typical room-temperature diffraction pattern of PpTA ($\sim$290 K) in which the major reflections are indexed. It should be noted that the right hand-side of the diffraction pattern is shadowed by the deformation rig's support structure.

Data analysis

Diffraction data analysis was carried out using the Fit2D software application in combination with specialized programs designed for automated processing [15, 16]. Each diffraction pattern was spatially corrected to account for detector non-linearity and geometrically corrected for the experimental geometry. To determine the radial positions of equatorial reflections, an arc-slice of the 110 reflection was first generated by radial integration and the scattering profile fitted using a pseudo-Voigtian function. A further azimuthal integration was then performed around each

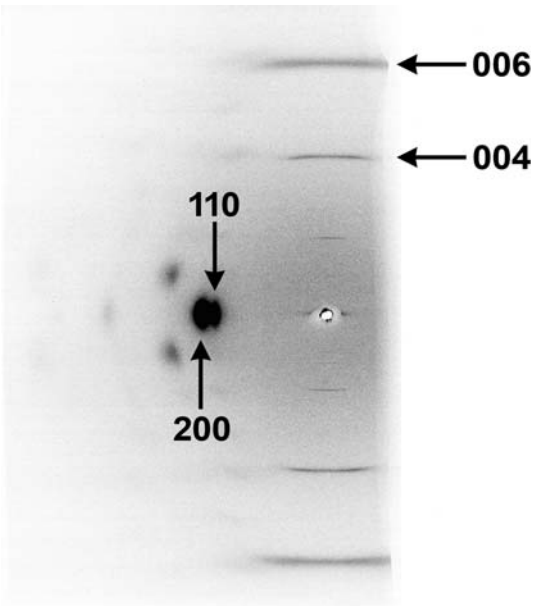

Fig. 1 Indexed diffraction pattern of PpTA at room temperature

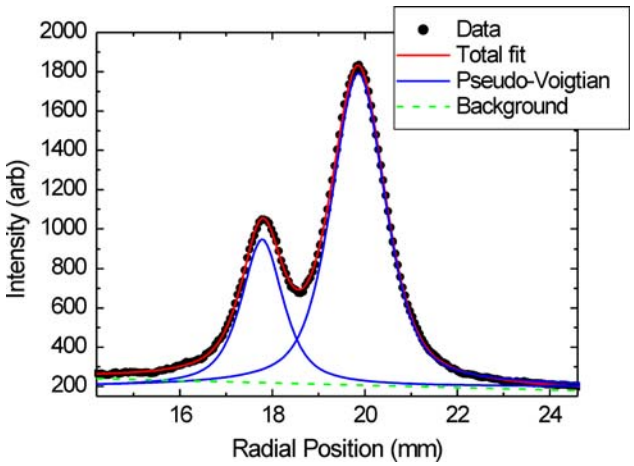

Fig. 2 Typical model fit to the radial scattering profile of the 110 and 200 reflections

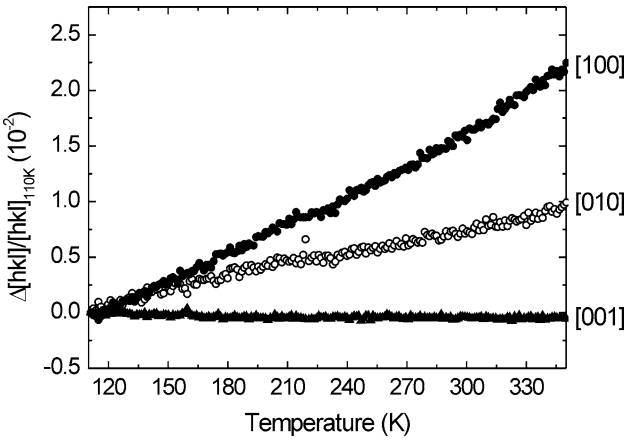

Fig. 3 Change in PpTA unit cell dimensions as a function of temperature over the range 110–350 K

azimuthal intensity maxima, using an azimuthal range of ±2°. The resulting radial profile was fitted using two pseudo-Voigt functions on a first order polynomial background to determine the radial positions of the 110 and 200 reflections. An example of a typical radial fit to the 110 and 200 scattering profile is shown in Fig. 2.

A similar approach was used to determine radial positions of meridional reflections. First the azimuthal centre of each 001 layer was obtained by integration and fitting. This was then used as the basis for a second integration operation to derive radial scattering profiles of the 004 and 006 layer lines which could be individually fitted with Gaussian functions.

From the radial positions of equatorial and meridional reflections, Bragg theory was used to determine lateral and axial crystal plane spacings (*d*-spacings and *c*-spacings, respectively). From these dimensions, the unit cell parameters for PpTA can be derived, where the lengths of the *a* and *b* axes are given by $a = 2d_{200}$ and $b = [{d_{110}}^{-2} - (2d_{200})^{-2}]^{-1/2}$ [6]. This calculation assumes a pseudo-orthorhombic unit cell symmetry ($\gamma = 90°$). It should be noted that finite temperature simulations have suggested that γ may vary by 0.2° for a 200 K increase in temperature [10]. Since this angular change is relatively small, however, simplification to a constant unit cell angle seems acceptable.

Results and discussion

PpTA lattice distortions with temperature

Assuming a pseudo-orthorhombic unit cell ($\gamma = 90°$), diffraction data collected from the undeformed fibre (at 289 K, prior to thermal annealing) yields lattice parameters of $a = 7.77$ Å, $b = 5.22$ Å and $c = 12.9$ Å. These are in good general agreement with literature values for PpTA [12, 17–19]. Figure 3 shows the change in PpTA lattice parameters as a function of Cryostream temperature. Lattice distortions are expressed in the form $\Delta[hkl]/[hkl]_{110K}$, where [hkl] defines a particular unit cell direction. The data shown corresponds to a single heating cycle from 110 to 350 K at a rate of 350 K/h. Diffraction patterns were acquired at approximately 12 s intervals (10 s of exposure and 2 s detector readout).

Figure 3 reveals that lattice parameter variations are comparatively linear across the temperature range under study. The PpTA crystal lattice expands transversally as temperature increases, corresponding to an increase in the area of the unit cell basal plane. The *c*-axis, meanwhile, shows only a very slight contraction. From the variations in PpTA unit cell length, the change in unit cell volume with temperature can also be derived, as shown in Fig. 4. As the calculation is based upon the data shown in Fig. 3, it intrinsically assumes a fixed pseudo-orthorhombic unit cell ($\gamma = 90°$). Figure 4 reveals that unit cell volume increases as temperature increases, in agreement with similar plots presented within the literature [8, 9].

From lattice parameter changes with temperature, thermal expansion coefficients (α) can be calculated for the three PpTA unit cell axes. Although the data shown in Fig. 3 appears relatively linear, the influence of non-linear heating cannot be completely discounted. Like most heating devices, the type of device used in this study ramps up to the chosen heating rate. Similarly, as the target temperature approaches, the ramp down is non-linear to avoid overshooting. To ensure that such effects do not influence the results of this study, the initial and final sections of the heating cycle shown in Fig. 3 will be neglected. Thus, thermal expansion coefficients for the PpTA crystal lattice are derived from linear fits to a constrained temperature range of 180–300 K.

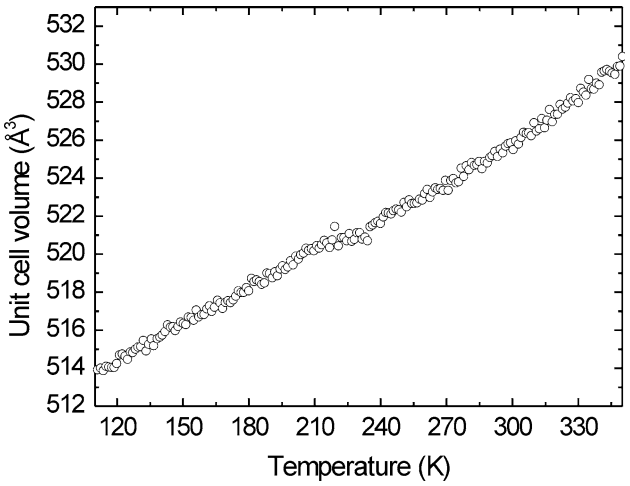

Fig. 4 PpTA unit cell volume changes with temperature

The coefficients of thermal expansion for the *a* and *b* unit cell axes are 8.89 and 2.94 × 10^{-5} K^{-1}, respectively. Despite the slight contraction that is apparent in Fig. 3, the *c* unit cell axis shows no statistically significant change. Differences between [100] and [010] can be explained in terms of a difference in lateral chain interactions. Whilst there are only van der Waal's forces acting along [100], the *b* unit cell axis is parallel to the direction of hydrogen bonding between amide groups on adjacent chains. The higher lattice modulus along the direction of hydrogen bonding translates into constrained thermal expansion along the *b* axis. A similar explanation also accounts for the lack of any dimensional change along the chain direction. This direction of the PpTA lattice exhibits the highest modulus due to strong intramolecular bonds. Indeed, it is precisely this feature that contributes to the fibre's remarkable mechanical properties. This stiffness acts as a barrier to thermal expansion/contraction, meaning that temperature predominantly influences lateral molecular interactions in PpTA rather than distorting the polymeric repeat length.

Whilst not directly related to the subject of thermal expansion coefficients, it is interesting to note that *a* and *b* unit cell lengths at 289 K in Fig. 3 are slightly larger than those recorded prior to the start of the experiment ($a = 7.79$ Å and $b = 5.23$ Å versus $a = 7.77$ Å and $b = 5.22$ Å). Whilst the difference may be small in absolute terms, it nevertheless shows that a temperature cycle can induce a permanent structural change (thermal annealing). It therefore reiterates the importance of an initial preconditioning step before data collection.

Comparisons with previous studies—part 1

Lateral lattice parameter variations shown in Fig. 3 are in good general agreement with trends observed in the literature. A number of studies report shrinkage of the unit cell's basal plane during cooling, and/or expansion during heating [6, 8, 9]. In all cases they observe a greater expansion/contraction along the [100] direction compared to [010]. The lack of any significant change in axial lattice spacings is also in good agreement with literature for low temperature experiments. The almost constant *c*-spacing is consistent with Iyer et al. [9], who failed to record any statistically significant axial change. They also observed a permanent increase in both basal plane axes following a cooling cycle, in agreement with the effects of thermal annealing seen in this study [9].

Thermal expansion coefficient values corresponding to previous studies are collected in Table 1 for comparison with the results of this study [6, 9, 10]. Table 1 shows that the results obtained for the *a* and *b* unit cell axes are in good agreement with theoretical values presented by Lacks and Rutledge [10]. There is also a good correlation with experimental results reported by Ii et al. [6]. For this latter comparison it is perhaps worth noting that their data were also collected following an initial thermal annealing step, although the actual temperature range they studied was around 200 K higher [6]. Whilst lattice distortions along the *a* and *b* unit cell axes seem to agree with literature values, a difference is found for the *c* axis. Calculations by Lacks and Rutledge [10] predict a contraction along the axial direction, predominantly as an elastic response to transverse expansion. Such a contraction, albeit less pronounced, has been reported experimentally by Ii et al. [6] but is not apparent in the present data. Whilst a convenient explanation would be the higher temperatures studied by Ii et al. [6] compared to this study, the calculations by Lacks and Rutledge [10] specifically reject this possibility (showing axial contractions are expected right down to 0 K). The reason for this difference therefore remains unclear, although it should be noted that other studies have reported similar results and qualified them simply as the difference between heating and cooling, without providing

Table 1 Summary of thermal expansion coefficients collected from literature sources (units 10^{-5} K^{-1})

	Present study	Iyer et al.[a]	Iyer et al.[b]	Ii et al.[c]	Ii et al.[d]	Lacks and Rutledge[e]
α_a	8.89	8.02	6.98	8.3	12.0	7.9
α_b	2.94	1.18	1.17	4.7	6.3	2.9
α_c	0	−0.12	0.61	−0.29*	−0.29*	−0.57

[a] Data derived for a 50 K decrease in temperature from 297 K

[b] Data derived for a 100 K decrease in temperature from 297 K

[c] Data derived during heating from 300 to 500 K

[d] Data derived during heating from 500 to 700 K

[e] Calculated values over the temperature range 300–500 K

* Data derived during heating from 300 to 600 K

any further explanation [9]. It is also possible that such small lattice parameter changes are beyond the experimental resolution (dictated by the detector pixel size, point-spread-function and sample-to-film distance).

A meaningful comparison between thermal expansion coefficients derived in this study and those reported previously is complicated by the range of values apparent in the literature. For example, α_b values range from 1.17 to 6.3 $\times$ 10^{-5} K^{-1}, whilst values for the *c* unit cell axis range from 6.1 $\times$ 10^{-6} K^{-1} to -3.6×10^{-5} K^{-1} [8, 9]. Although the reliability of previous studies cannot be independently verified, it is worth considering experimental differences that may influence the reported results. One key difference between this study and previous studies is the number of data points used to calculate thermal expansion coefficients. The data shown in Fig. 3 contain 213 individual data points with more than 100 points falling in the 120 K range used to calculated thermal expansion coefficients. By comparison, data presented by Ii et al. and Iyer et al. contain only 8 and 3 measurement points, respectively. Using fewer data points increases experimental error as the weighting of individual values increases. Another important difference between this study and previous studies is in the type of sample used. The present experimental work was performed on a single PpTA fibre rather than on fibre bundles (employed in all previous studies). The use of a single fibre (measuring approximately 12 μm in diameter) eliminates the averaging effects inherent to measuring hundreds of individual fibres simultaneously. For example, it is notoriously difficult to achieve uniform stress when preparing fibre bundles. This can lead to a distribution in stress-induced lattice strain within the sampling volume. Fibre bundles are also significantly larger than single fibres which can result in turbulent air flows during cooling with Cryostream devices. This can cause heterogeneous sample cooling and the formation of ice crystals, as noted by Iyer et al. [9]. The only potential drawback in the present experimental method is in the use of an X-ray microbeam that is significantly smaller than the fibre diameter. This risks data collection from highly localized heterogeneities within the fibre and makes alignment between the fibre and X-ray beam more critical. Such uncertainty could be eliminated completely by carrying out data collection in a scanning acquisition mode for future studies.

The influence of applied macroscopic stress

In order to investigate the interplay between temperature and applied stress, Fig. 5 shows the variation of PpTA lattice parameters as a function of temperature for the same fibre under two different loading conditions. The first series represents the undeformed fibre at nominal load, and was previously used to calculate the thermal expansion coefficients shown in Table 1. The second series shows the same temperature range, but with the fibre being held at a constant 2% macroscopic strain. Assuming a typical PpTA fibre diameter of 12 μm, the force registered on the load cell corresponds to an applied macroscopic fibre stress of 2.56 GPa. For deformation under a perfectly elastic regime, this would be equivalent to a tensile modulus of 128 GPa, in agreement with literature values for Kevlar49 [14]. All diffraction patterns were collected using 10 s exposures during heating from 110 to 350 K at a rate of

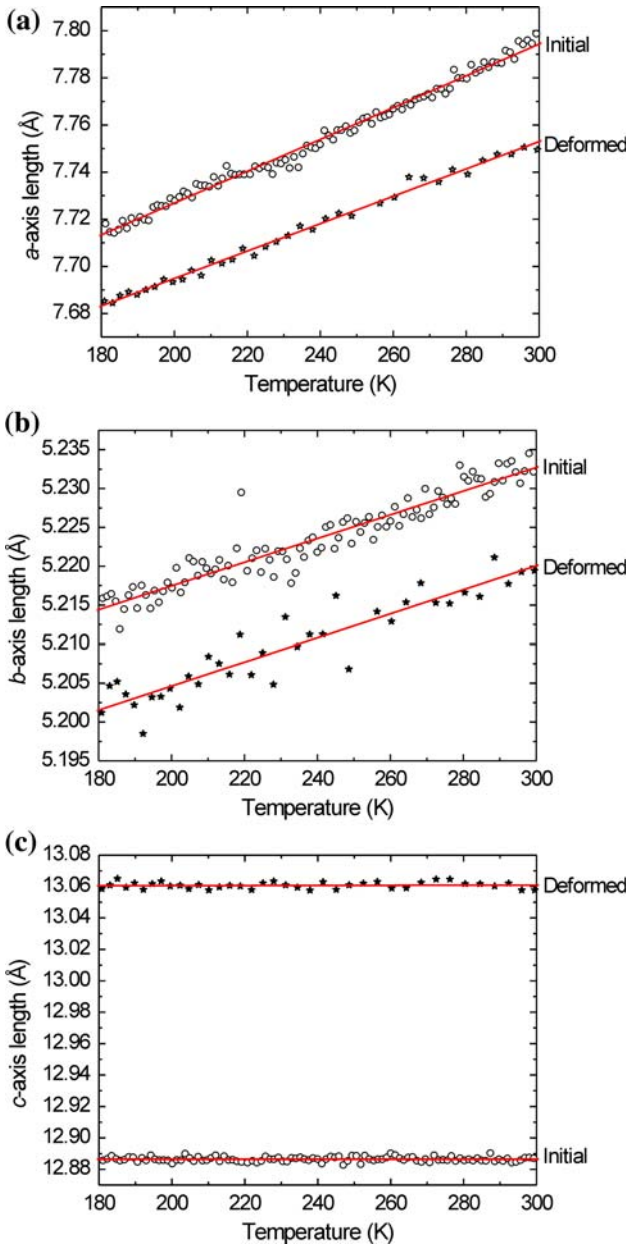

Fig. 5 Variation of PpTA unit cell dimensions with temperature for the same fibre at 0% (initial) and 2% (deformed) applied macroscopic strain

350 K/h. As before, only data within the range 180–300 K will be considered in order to avoid possible influence from non-linear heating.

From its initial undeformed state, axial tension applied to the macroscopic fibre results in a significant increase in the *c* unit cell dimension. Based upon average values from Fig. 5, this corresponds to an axial crystal lattice strain of 1.35%. The equivalent crystal modulus (assuming uniform stress) is 189 GPa. This is in good agreement with values reported in literature, which fall within the range 168–214 GPa [7, 12, 20–23]. Whilst the axial *c* dimension of the PpTA crystal lattice increases, the unit cell's lateral dimensions contract. This corresponds to average transverse crystal strain values of −0.51% and −0.26% for the *a* and *b* unit cell axes, respectively. This basal plane shrinkage during the application of axial tension is the inverse behaviour to that observed with increasing temperature. Just as modelling predicts an axial contraction with increasing temperature as an elastic response to basal plane expansion, basal plane shrinkage can be attributed to the elastic response to axial lattice strain bringing chains closer together. The smaller contraction observed along the [010] direction compared to [100] is the result of hydrogen bonding along the *b* unit cell axis which increases the lattice modulus in this direction, thus limiting chain movement.

Thermal expansion coefficients calculated from the data shown in Fig. 5 are collected in Table 2. As in the previous case, thermal expansion coefficients were derived from linear fits to the experimental data over the temperature range 180–300 K (the fits are shown in Fig. 5). The results in Table 2 reveal that axial deformation primarily influences the α_a parameter, decreasing it by around 15% to 7.67×10^{-5} K^{-1}. In contrast, there is very little change in the coefficients of thermal expansion for the other unit cell axes. A third column has also been included in Table 2, corresponding to the same fibre in an unloaded state (a nominal stress of 0.37 GPa). This latter set represents a fibre which has undergone both heating and deformation cycles. Despite the change in α_a under deformation, upon the removal of applied stress it returns to almost its original value. This seems to confirm that the slight reduction in thermal expansion along [100] under an applied axial stress is the result of an elastic response to axial lattice distortion.

Table 2 Thermal expansion coefficients derived from linear fits to lattice parameter changes with temperature from the same fibre at different loading levels (units 10^{-5} K^{-1})

	Initial	Deformed	Relaxed
α_a	8.89	7.67	8.97
α_b	2.94	2.98	2.87
α_c	0	0.02	−0.09

In terms of the *b* unit cell axis, there is a slight decrease in α_b after tension has been removed, whilst thermal expansion along *c* becomes negative. The significance of this negative α_c result is difficult to judge without being able to categorically discount the influence of time dependent compliance.

The results in Fig. 5 and Table 2 demonstrate that any thermally induced changes in *c*-spacing are insignificant compared to axial lattice distortions due to applied macroscopic stress. By contrast, although lateral crystal strain due to axial deformation changes the overall lattice spacing, the magnitude of any temperature-induced lattice change is limited (with only a 15% decrease in α_a). This indicates that the stresses involved in thermal lateral expansion/contraction of the unit cell dominate those arising due to the application of axial tension.

Comparisons with previous studies—part 2

In order to put these results into context, the interplay between temperature and applied axial stress needs to be considered alongside previous studies. Ii et al. [7] demonstrated that PpTA lattice strain along the chain axis varies as a function of temperature over the range 300–600 K. They recorded higher strains for the same applied stress as temperature increases, although they did not report on associated lateral changes of the unit cell [7]. Their experimental observations are also backed up by the theoretical calculations of Lacks and Rutledge [10]. These predict the Young's Modulus of PpTA to decrease as temperature increases, with a reduction of around 10% between 100 and 400 K [10].

In terms of the present results, the variations reported by Ii et al. and Lacks and Rutledge [7, 10] would be equivalent to a greater coefficient of thermal expansion along the *c* direction during heating under applied strain. This result can be observed in Table 2, where the α_c parameter increases by 0.02×10^{-5} K^{-1}. The overall change is relatively small, however, corresponding to a decrease in lattice modulus with increasing temperature of only 3.2×10^{-3} GPa K^{-1}. By comparison, Ii et al. report a decrease of around 1.0×10^{-1} GPa K^{-1} whilst the value calculated by Lacks and Rutledge is 7.0×10^{-2} GPa K^{-1} [7, 10]. The present results are therefore more than an order of magnitude smaller than the nearest published value.

Iyer et al. [9] previously attributed a lack of axial lattice contraction in data collected below room temperature to the temperature range under study. Whilst no attempt has been made to identify the mechanism behind this, a similar explanation may also explain the relative insensitivity of lattice strain to temperature, as shown in Table 2. One significant influence could be the role of torsional energy during the deformation of PpTA chains. In the crystal

structure of PpTA, the phenyl rings are locked in place by adjacent chains. In this interlocking configuration the phenyl rings cannot rotate during deformation. As temperature increases, the polymer chains move further apart due to thermal expansion, as demonstrated by the increasing lateral lattice parameters in Fig. 3. This increases the rotational freedom of the phenyl rings, which corresponds to a decrease in axial modulus [10].

Figure 5 reveals that reducing temperature and the application of axial strain both result in a reduction in lateral chain spacing. In the latter case, the 2% applied strain is equivalent to a temperature decrease of around 70 K. The resulting reduction in inter-chain distance corresponds to less rotational freedom for phenyl rings during subsequent deformation. This could account for the difference between the present results and previous studies, provided the impact of increased phenyl ring rotations on mechanical properties only starts to become significant above a critical inter-chain spacing. This latter provision is not supported by the calculations of Lacks and Rutledge [10]. On the other hand, if this provision did not exist, elastic modulus would be expected to increase systematically as applied strain increases due to enhanced locking of the crystal structure.

From the change in lateral lattice parameters during deformation, longitudinal Poisson's ratio of the PpTA crystal lattice can be estimated [24]. Moreover, using the linear model fits shown in Fig. 5, the temperature dependence of longitudinal Poisson's ratio can be determined. The result is shown in Fig. 6 for the [100] and [010] lattice directions. It reveals that whilst the [100] Poisson's ratio varies significantly with temperature, the value along *b* remains relatively constant. Again, this can be attributed to enhanced dimensional stability along [010] due to hydrogen bonding. The resulting 'room temperature' values of $\upsilon_{lt} = 0.38$ for [100], and $\upsilon_{lt} = 0.18$ for [010] are in reasonable agreement with values reported by Nakamae et al. [24] (0.31 and 0.2, respectively).

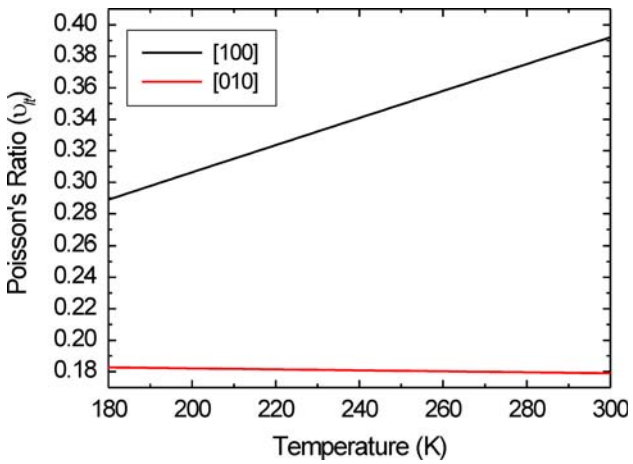

Fig. 6 Variation in longitudinal Poisson's ratios along [100] and [010] with temperature

Conclusions

The results of this study reveal a number of interesting features of the relationships between PpTA lattice parameters and temperature. All unit cell axes exhibit linear thermal expansion behaviour which is greatest along the [100] direction whilst being reduced along [010] by inter-chain hydrogen bonding. Thermal expansion coefficients are found to be 8.89 and 2.94 $\times$ 10^{-5} K^{-1} for the *a* and *b* unit cell axes, respectively, with no significant change along the *c* unit cell direction. The results are in general agreement with a number of previous studies although no axial contraction was observed in this particular case.

Regarding the effect of both applied strain and temperature, in some respect the present work appears to raise more questions than it does provide answers. Crystal strain dominates with respect to axial lattice distortions induced by temperature changes, with only a small change in the [100] coefficient of thermal expansion under an applied strain. The impact of phenyl ring locking and its proposed effect on axial lattice strain seems plausible given differences between the different studies. This hypothesis could be tested by further experiments investigating the effect of temperature and strain in much greater detail. By studying lattice distortions over a range of different temperatures and strain levels, it should be possible to decouple the different contributions. This might lead to a better understanding of how bulk mechanical properties in PpTA are influenced by inter-chain interactions.

Whilst this work is predominantly a study of PpTA lattice distortions, the results also highlight the benefit of combining multiple in situ techniques, such as cryo-cooling and deformation.

References

1. Liu X, Yu W (2006) J Appl Polym Sci 99:937
2. Duband L, Hui L, Lange A (1993) Cryogenics 33(6):643
3. Pereira JM, Roberts GD, Revilock DM (1997) NASA technical memorandum 107532
4. Strife JR (1979) J Compos Mater 13(4):264
5. Rojstaczer S, Cohn D, Marom G (1985) J Mater Sci Lett 4:1233
6. Ii T, Tashiro K, Kobayashi M, Tadokoro H (1986) Macromolecules 19:1772
7. Ii T, Tashiro K, Kobayashi M, Tadokoro H (1987) Macromolecules 20:347
8. Jian A, Vijayan K (2003) Curr Sci 78:331
9. Iyer RV, Sooryanarayana K, Guru Row TN, Vijayan K (2003) J Mater Sci 38:133. doi:10.1023/A:1021178219377

10. Lacks DJ, Rutledge GC (1994) Macromolecules 27:7197
11. Riekel C, Dieing T, Engstrom P, Vincze L, Martin C, Mahendrasingam A (1999) Macromolecules 32:7859
12. Davies RJ, Burghammer M, Riekel C (2006) Macromolecules 39:4834
13. Davies RJ, Koenig C, Burghammer M, Riekel C (2008) Appl Phys Lett 92:101903
14. Rao Y, Waddon AJ, Farris RJ (2001) Polymer 42:5937
15. Davies RJ (2006) J Appl Crystallogr 39:262
16. Davies RJ (2006) J Appl Crystallogr 39:267
17. Lui J, Cheng SZD, Geil PH (1996) Polymer 37:1413
18. Northolt MG (1974) Eur Polym J 10:799
19. Tashiro K, Kobayashi M, Tadokoro H (1977) Macromolecules 10:413
20. Tashiro K, Kobayashi M (1991) Polymer 32:454
21. Slutsker LI, Chereiskii ZY, Utevskii LY, Kuzmin VN, Kalmykova VD, Sokolova TS, Volokhina AV, Kudryavtsev GI (1975) Polym Sci USSR 17:1808
22. Kotera M, Nakai A, Saito M, Izu T, Nishino T (2007) Polym J 39:1295
23. Northolt MG, van Aartsen JJ (1977) J Polym Sci Polym Symp 58:283
24. Nakamae K, Nishino T, Xu AR (1992) Polymer 33:4898